International Journal of GEOMATE, Aug., 2024 Vol.27, Issue 120, pp.27-39
ISSN: 2186-2982 (P), 2186-2990 (O), Japan, DOI: https://doi.org/10.21660/2024.120.4393
Geotechnique, Construction Materials and Environment

SOME INSIGHTS INTO THREE-DIMENSIONAL MODELING OF TUNNEL EXCAVATION

*Khoo Chee Min[1], Hisham Mohamad[1] and Phromphat Thansirichaisree[2]

[1]Department of Civil & Environmental Engineering, Universiti Teknologi PETRONAS, Malaysia; [2]Department of Civil Engineering, Thammasat University, Thailand

*Corresponding Author, Received: 19 Jan. 2024, Revised: 24 May 2024, Accepted: 25 May 2024

ABSTRACT: For today's demands in underground infrastructure, geotechnical considerations are gaining prominence, emphasizing the resolution of complex problems through numerical modeling and soil-structure interaction analysis. There is a clear trend shifting away from two-dimensional (2-D) plane strain or axisymmetric idealizations to the comprehensive analysis of full three-dimensional (3-D) models. However, despite the inclination towards 3-D modeling of tunnels, establishing a realistic 3-D model for this purpose remains a time-consuming process. This typically involves multiple iterative and incremental phases, essential for gaining deeper insights into the three-dimensional nature of the problem. Beyond selecting an appropriate constitutive soil model, realistically finite element modeling and accurate simulation of the tunneling process are of paramount importance. This study focuses on the development of a practical full 3-D model and simulation of the Earth Pressure Balance (EPB) shield tunneling process using the finite element code PLAXIS 3D. The numerical model incorporates tunnel boring machine driving data recorded during tunnel construction and is validated through back-analysis of field measurements of tunneling-induced ground surface settlements. The findings demonstrate that numerical simulation can realistically reproduce the main characteristics of EPB shield tunneling. The study recommends adopting non-linear face pressures with depth based on the analysis of tunneling data. Regarding grouting pressure, an effectively linear distributed pressure may be considered, accounting for the grout weight and the increase of soil stresses with depth. This validated numerical framework provides valuable guidance for researchers and practitioners to construct more efficient, reliable, and accurate 3-D models.

Keywords: Numerical simulation, 3-D modeling, Finite element analysis, Back analysis, EPB tunneling process

1. INTRODUCTION

In response to today's demands for underground infrastructure, geotechnical considerations are taking center stage, with a focus on resolving complex problems through numerical modeling and the analysis of soil-structure interactions. A noticeable trend is the shift from problems traditionally confined to two-dimensional (2-D) plane strain or axisymmetric idealizations to the analysis of full three-dimensional (3-D) models. The utilization of 3-D modeling and analysis often yields more representative results and, consequently, more realistic solutions. The challenge lies in finding the optimum balance between analysis accuracy, required complexity, and the associated time and cost of design analysis.

Tunnel construction is inherently three-dimensional and time-dependent. The distribution of stresses and the evolution of ground movements around an advancing tunnel occur in three dimensions and over time. Finite element (FE) analysis presents significant opportunities for modeling and simulating tunnel construction. The preference for 3-D modeling of tunnels has grown due to recognized limitations of 2-D modeling [1,2] and the ability of 3-D modeling to better capture responses of tunnel excavations [3]. Advances in large-scale computing resources have facilitated notable progress in FE modeling in recent years. Literature reports various instances of 3-D finite element simulations of tunnels [4-20]. Nevertheless, the development of routinely applicable realistic 3-D finite element analysis remains a prolonged process, typically involving multiple iterative and incremental phases to ensure reliability and accuracy while minimizing computational efforts. In addition to selecting a suitable constitutive soil model, the optimization of finite element modeling and the simulation of the tunneling process is of utmost importance.

This paper presents the development of a comprehensive 3-D model and outlines the primary modeling techniques used to simulate the Earth Pressure Balance (EPB) shield tunneling process, employing the finite element code PLAXIS 3D. Field measurement data from the Klang Valley Mass Rapid Transit (KVMRT) Kajang Line tunnels in Kuala Lumpur, Malaysia, was utilized to calibrate and validate the model. Numerical back-analysis was conducted using the tunnel boring machine (TBM) driving data recorded during tunnel construction. The objective of this paper is to enhance understanding of key issues affecting 3-D modeling, thereby providing recommendations and guidance for researchers and practitioners to construct more efficient, reliable, and accurate 3-D models.

2. RESEARCH SIGNIFICANCE

This research marks a significant advancement in the state of the art of 3-D modeling of tunnel excavation, particularly for the EPB shield tunneling process. By developing and validating a comprehensive 3-D model using PLAXIS 3D, the study addresses the limitations of traditional 2-D models, providing a more realistic simulation of tunneling processes. Incorporating real-time tunnel boring machine driving data and conducting rigorous back-analysis, this work offers a validated framework that enhances the accuracy and reliability of 3-D models. This breakthrough provides valuable insights and practical guidance, setting a new standard for future underground projects.

3. LITERATURE REVIEW

More recently, there has been a remarkable development in the 3-D finite element modeling that encompasses essential components of tunnel boring machine, the tunneling process, nonlinear soil and structure characteristics, and intricate soil-structure interaction [13,15,17,21,22]. These models, introduced by various researchers, have each contributed unique aspects and numerical approaches to simulate shield tunneling [23].

Notably, Do *et al.* [13] conducted a 3-D numerical study on twin tunnels, incorporating important components of mechanized tunneling such as face pressure, shield weight, and grout-filled gaps. Typically, face pressure is simulated by a horizontal load at the interface between the TBM and the excavated soil, often presented as a triangular or uniform distribution [11,19,20]. Additionally, Kavvadas *et al.* [16] presented a 3-D numerical model employing advanced techniques to simulate the shield-ground interface, time-dependent grout setting, and the configuration and stiffness of segmental lining joints. Chortis *et al.* [24] highlighted the significance of face pressure on surface settlements, emphasizing its dependence on the geometrical gaps between the TBM cutter head and the final lining. Various causes of the annular gap were identified, including the cutter head overcut, shield conicity, and the installation of the segmental lining within the shield. The shield conicity has been explicitly modeled by researchers [8,9,16].

Numerical simulation methods proposed by Kasper and Meschke [8], Zhao *et al.* [10], and Lambrughi *et al.* [11] share similarities, with Lambrughi *et al.* [11] particularly introducing a model for the steering gap using a thin layer of continuous linear elastic elements and simulating grout pressure with continuum elements. Meanwhile, Litsas *et al.* [14] investigated the influence of the tail shield gap in mechanized tunneling via parametric analyses, while Nagel and Meschke [25] utilized a finite difference method to simulate backfill pressure distribution. In specific cases, a uniform distribution grouting pressure has been adopted, as observed in the works of Fargnoli *et al.* [15], Founta *et al.* [19], Kavvadas *et al.* [16], Lambrughi *et al.* [11]. Nikakhtar *et al.* [18] delved into the grout material hardening process through gap grouting modeling.

Segmental lining, conventionally modeled as a continuous cylindrical shell with no joints, has evolved significantly over time. Muir Wood [26] first proposed a monolithic ring model, which laid the foundation for further improvements. Subsequently, Arnau and Molins [27] incorporated spring elements to simulate the interaction between the lining and surrounding ground. Building upon these advancements, Do *et al.* [12] presented a 3-D model of segmental lining with linear elastic shell elements and rotational springs for joint simulation.

Several publications on numerical modeling of tunnels address mesh optimization, considering model size, grid refinement, and order of elements [13,17,28]. Table 1 summarizes recommendations for numerical model size based on various studies carried out by previous researchers. Notably, Möller [3] proposed expressions for model dimensions for shallow tunnels, while Vitali *et al.* [17] emphasized the need to consider factors such as initial stresses and geological features, which are often overlooked in existing recommendations. It was noted that linear bricks or tetrahedral elements were mainly used to model the lining, the TBM shield, and the grout [23].

Table 1 Recommendations for numerical model size by previous researchers

Reference	Model Size	Remarks
Meisnerr [29]	4D to 5D	Width
Möller [3]	5D	Width from opening
Lambrughi *et al.*	H + 4D	Height
[11]	2 (H + 4D)	Length
	2 (H + 4D)	Width
Vlachopoulos and	6D	Width from opening
Diederichs [30]	$3R_{yield}$	Width from plastic zone
Vitali *et al.* [17]	5.5D	Width (linear material)
	16D	Width (nonlinear mat.)
	$1D^f + 3D^b$	Additional length
Ramsheh *et al.*	H + 4D	Height
[31]	10D	Length
	5D	Half model width

Note: H = depth of tunnel; D = tunnel diameter; R_{yield} = yield radii; f = from the front boundary; b = from the back boundary

In a nutshell, the complexity of simulating the shield tunneling procedure stems from several factors, including the 3-D geometry, variations in face pressure, the presence of gaps between the shield and the surrounding ground (such as cutter head overcut, conical or telescopic-shaped shield and annular void),

the grout injection pressure and its time-dependent consolidation behavior, and the structural system of the segmental lining. As highlighted by Kartz *et al.* [23], certain crucial TBM driving parameters can be explicitly incorporated into 3-D finite element simulations.

4. METHODOLOGY

4.1 TBM Driving Parameters

The selected case study for EPB tunneling involves a 2.7 km-long stretch from Semantan North Portal to Pasar Seni Station in the KVMRT Kajang Line project [32]. This study focuses on twin bored tunnels constructed using two EPB machines, with key technical data provided in Table 2.

Table 2 Key technical data of the EPB machine

Description	Data
Machine type	EPB shield
Length TBM + back-up	120 m
Weight TBM + back-up	645 ton
Working pressure (at axis)	5 bar
Front shield diameter (without hard facing)	6.630 m
Front shield length	2.815 m
Center shield diameter	6.620 m
Center shield length	2.575 m
Tail skin diameter	6.610 m
Tail skin length	3.850 m
Thrust cylinder	22 nos.
Total thrust force	4742 ton

Back analyses were performed through three-dimensional finite element simulation of the EPB shield tunneling process, utilizing the recorded TBM driving data for the section of tunnel advance between -10D and 10D from the monitoring section at Chainage 1+960, where D represents the tunnel diameter. Negative values indicate the TBM's location before reaching the monitoring section. This location can appropriately be considered a greenfield tunneling scenario. The tunnel cover-to-diameter (C/D) ratio ranged from approximately 1.8 to 2.2, with a lateral separation of 12.7 m between the centerlines of the side-by-side twin tunnels. The study utilized high-quality monitoring data from a series of ground settlement markers (GSM1962 to GSM1967) positioned along this monitoring section.

Fig.1 illustrates the overall subsurface conditions, which exhibit a consistent division of two distinct sub-divisions based on the Standard Penetration Test (SPT) value of 50. The overlying fill and residual soils typically reach a depth of 8 m below the ground surface level. The tunnels are situated below this layer, encountering the hard-weathered materials (SPT ≥ 50) of the Kenny Hill Formation. Groundwater tables were measured at depths ranging from 2 to 3 m below ground level.

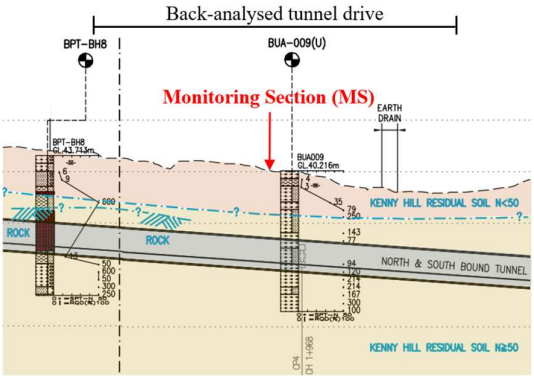

Fig.1 General subsurface conditions

The TBM primarily operated in closed mode during its drives. Key driving data, such as face support pressures, tail skin grouting pressures, and advance thrust forces, were collected from the TBM data logger and daily operating sheets. These data records were averaged on a ring basis for assessment.

The pressures of the soil paste in the excavation chamber (i.e. face support pressures) were extracted from six earth pressure sensors positioned over the cutter head. Fig.2 presents the individual point pressures recorded, which were analyzed to establish a representative support pressure profile and gradient for each ring built in the numerical simulation.

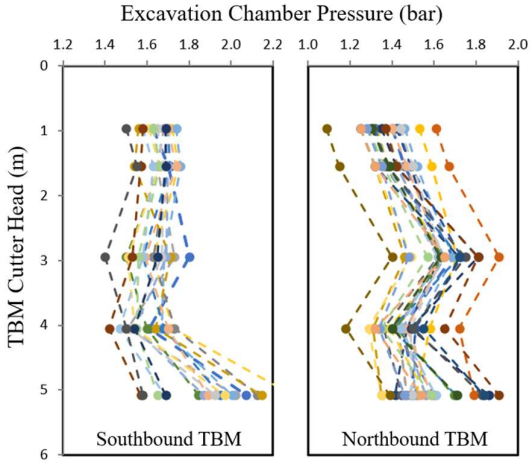

Fig.2 Records of excavation chamber pressures

Statistically, the average face support pressures ranged between 1.27 and 1.80 bar as the Northbound (NB) TBM progressed, while slightly higher average pressures of 1.52 to 1.95 bar were recorded for the Southbound (SB) TBM. A high penetration of more than 20 mm/rev, with an average production rate of

9.8 m advance per day with a maximum production of 19.6 m/day were reported by Chin *et al.* [33].

A two-component injection system, consisting of component A and B, was utilized to simultaneously fill the annulus void behind the segments as the tunnel advanced. Component B, a liquid accelerator (sodium silicate), was introduced into the component A grout mix during injection into the annulus. As the amount of component B is less than 10% of the total volume, and its pressure was considered negligible [34]. Fig.3 illustrates the recorded grouting pressures across the four grout ports. Generally, the grouting pressures at the grout ports remain relatively constant throughout the tunnel drives, with localized fluctuations observed in the Southbound TBM. The grout pressure in the annulus void itself was not known.

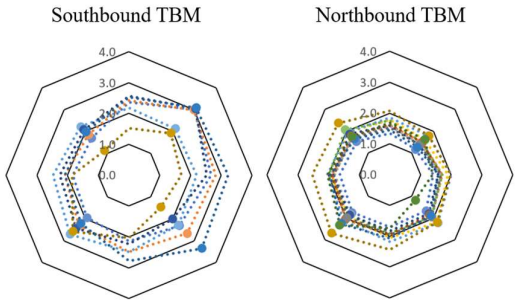

Fig.3 Records of tail skin grouting pressures at grout ports (bar)

Out of the 22 thrust cylinders, the typical range of total thrust force was approximately 10 – 14 MN, as depicted in Fig.4. Throughout the length of the tunnel drive, a slightly reduced advance thrust force was employed when the Southbound TBM traversed the shallower cover area directly beneath a surface earth drain.

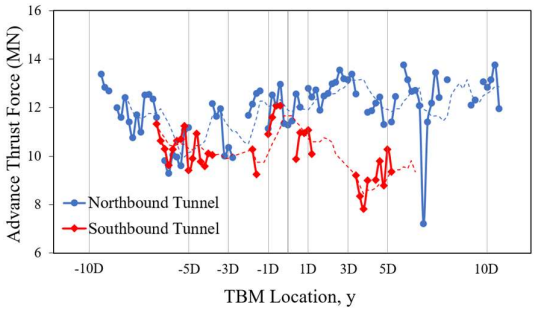

Fig.4 Records of advance thrust forces

4.2 Three-dimensional Numerical Model

The three-dimensional numerical modeling and back analysis were conducted using a commercially available finite element program, PLAXIS 3D [35]. This software facilitated the simulation of tunnel advancement in a manner closely resembling the processes occurring during actual tunnel excavation.

4.2.1 Model set-up and boundary conditions

A comprehensive 3-D model, considering a height of 40 m and a width of 80 m, was employed for the analysis. The model has a length of 130 m, with the first 42 m of tunnels modeled using the "all-in-once installation" approach [36], followed by a step-by-step simulation. These dimensions were chosen to ensure that there is no undue influence from the model boundaries. Lateral boundary fixity was applied perpendicular to the vertical plane, while both lateral and vertical fixities were assigned to the bottom of the model. Consequently, movements normal to the vertical boundaries and in all directions at the base are restrained. Fig.5 provides a perspective view of the developed numerical model, comprising 201,308 elements and 310,832 nodes. The model utilized a "medium" coarseness element distribution with 10-noded tetrahedral elements. The adequacy of the mesh density was assessed through iterative reruns with smaller mesh dimensions until displacement changes became insignificant [37,38], confirming that the current mesh is appropriate for the desired level of accuracy [39].

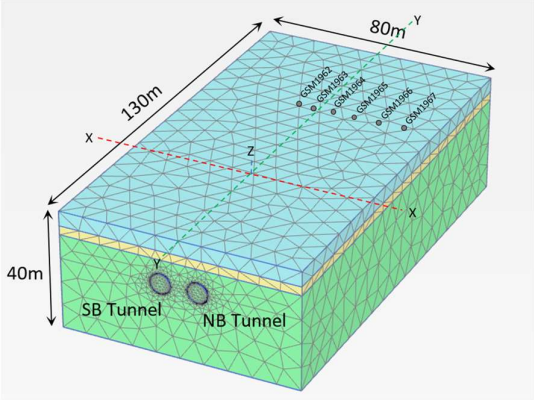

Fig.5 Perspective view of the developed 3-D model

4.2.2 Soil constitutive model and input parameters

The Hardening Soil with Small Strain Stiffness (HS-Small) model is an extension of the Hardening Soil (HS) model, encompassing nearly all its features [40]. Fundamentally, the HS model is derived from the hyperbolic model initially proposed by Duncan and Chang [41], with further enhancements to the hyperbolic formulations. For additional information, readers are directed to Schanz *et al.* [42].

In addition to the HS model, the HS-Small model introduces a formulation of small-strain stiffness properties, incorporating a high initial elastic stiffness of soils denoted by the very small strain shear modulus (G_0) stiffness degradation with increasing

Table 3 Soil parameters of the HS-Small model

Parameter (unit)	Notation	Fill	Kenny Hill Residual Soil	
			N = 30	N = 100
Soil type	-	SILT / CLAY	Sandy SILT	Sandy SILT
Drainage type	Model	Drained	Drained	Drained
Unsaturated unit weight (kN/m^3)	γ_{unsat}	18.0	19.0	20.0
Saturated unit weight (kN/m^3)	γ_{sat}	18.0	19.0	20.0
Secant stiffness (kN/m^2)	E_{50}^{ref}	8 x 10^3	60 x 10^3	200 x 10^3
Tangent stiffness (kN/m^2)	E_{oed}^{ref}	8 x 10^3	60 x 10^3	200 x 10^3
Unloading/reloading stiffness (kN/m^2)	E_{ur}^{ref}	24 x 10^3	180 x 10^3	600 x 10^3
Poisson's ratio	ν	0.2	0.2	0.2
Power for stress-level dependency of stiffness	m	0.5	0.5	0.5
Shear modulus at very small strain (kN/m^2)	G_0^{ref}	48 x 10^3	360 x 10^3	1200 x 10^3
Shear strain at $G_s = 0.722G_0$	$\gamma_{0.7}$	0.15 x 10^{-3}	0.12 x 10^{-3}	0.10 x 10^{-3}
Cohesion (kN/m^2)	c'^{ref}	5	10	15
Friction angle (°)	ϕ'	28	28	29
Dilatancy angle (°)	φ	0	0	0

strain in monotonic loading, and stress path-dependent stiffness, including the regaining of high stiffness after sharp loading reversals [43]. The HS-Small model describes this behavior using an additional strain-history parameter and two additional material parameters, G_0 and $\gamma_{0.7}$. The small strain threshold parameter $\gamma_{0.7}$ represents the shear strain level at which the secant shear modulus (G_s) is reduced to approximately 70% of G_0.

The soil parameters of HS-Small model, as outlined in Table 3, were derived from ground investigation data collected at the tunneling site. Triaxial loading/secant stiffness (E_{50}) was determined using a locally well-established correlation of E_{50}/N = 2, where N represents SPT blow counts [44].

Oedometer loading/tangent stiffness (E_{oed}) was taken as E_{50}, and unloading/reloading stiffness (E_{ur}) was set as $3E_{50}$ by default in PLAXIS. These stiffness parameters generally align with the calibrated HS parameters of residual soil from the Kenny Hill Formation, as presented in Govindasamy *et al.*'s study [45]. For the very small strain shear modulus (G_0) was empirically correlated with SPT blow counts of 12N based on the work by Veeresh *et al.* [46].

4.3 Simulation Procedures of Tunneling Process

The shield tunneling process is modeled using a step-by-step approach, with each excavation step corresponding to an advancement of the tunnel face by 1.4 m, which is equal to the width of a lining ring. The computation involves several construction steps in the shield tunneling process:

(1) Excavation and Support Pressure Application: This step involves excavating the ground at the tunnel face while simultaneously applying the necessary support pressure to prevent active failure at the face.
(2) Tunnel Lining Installation: This step models the installation of the tunnel lining.
(3) Jacking Force Application: Applying the jacking force to propel the TBM forward.
(4) Grout Injection: Injecting grout behind the segments to fill the gap between the soil and the newly installed lining.

These construction steps are iteratively applied as the TBM advances, ensuring a comprehensive simulation of the advancing tunnel construction process.

4.3.1 General characteristics of the shield TBM

Fig.6 provides a comprehensive overview of the components of the EPB machine and the pressures at the excavation face, shield, and around the lining. The shield, with a total length of 9.24 m and a thickness of 0.06 m, is designed with a varying diameter in the longitudinal direction as depicted in Table 2. The cutting head has a diameter of 6.67 m, allowing for a potential 0.02 m overcut at the tunnel face. The gap between the rear part of the machine (i.e. tail skin) and the tunnel lining is 0.07 m.

In numerical modeling, the structural components of the tunnel, such as the shield machine and lining, are presented as linear elastic materials using 10-node tetrahedral elements [23,47]. Solid shell elements, specifically curved plates, are employed to simulate the TBM and tunnel lining. Table 4 outlines the material properties of the structural plate representing TBM.

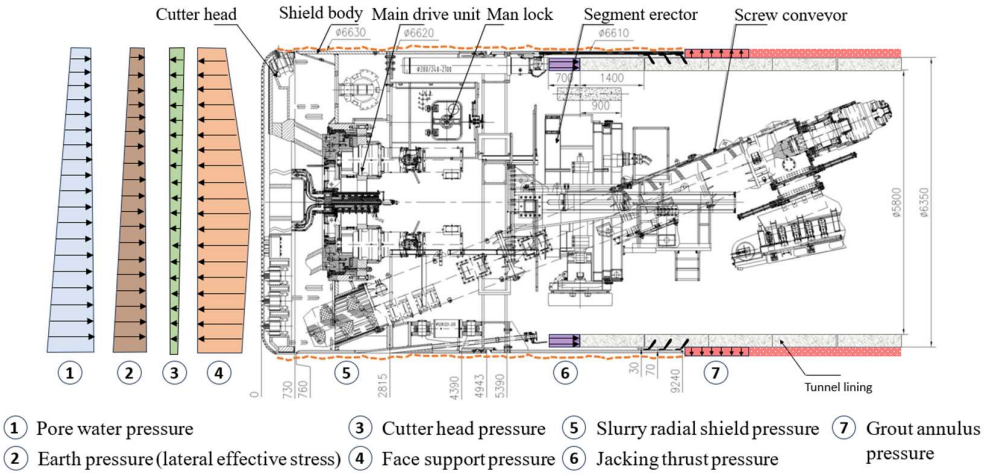

Fig.6 EPB machine components and the pressures surrounding the shield and lining

Table 4 Material properties – structural plate representing TBM

Parameter (unit)	Notation	Value
Material type	-	Elastic
Unit weight (kN/m^3)	γ	247
Isotropic	-	Yes
Young's modulus (kN/m^2)	E_{shield}	2 x 10^9
Poisson's ratio	ν	0
Thickness (m)	d	0.17
Shear modulus (kN/m^2)	G_{shield}	1 x 10^9
Interface strength reduction	R_{inter}	0.9

The total weight of the TBM, excluding the back-up train, is determined based on the weight per unit volume of the shield. This approach is justified as the study primarily focuses on the ground surface settlement generated by the shield tunneling. Additionally, uplift at the tunnel invert is more pronounced in shallow excavations and can be corrected using the Hardening Soil model, which accounts for higher soil stiffness in unloading/reloading conditions as soil is excavated by the TBM [16].

4.3.2 Modeling the shield-soil interaction

Various publications have proposed diverse methods to model the shield-soil interaction, including gap elements, interfaces, regions with reduced elastic modulus, etc. with some studies focusing on simulating the tail gap [8,10-12]. Kavvadas *et al.* [16] demonstrated the significant influence of the cutter head overcut and shield conicity on predicted ground surface settlement.

In this study, the shield was modeled with a simplified cylindrical-shaped geometry (constant diameter) instead of a conical shape. The gaps were geometrically defined and simulated by surface contraction (volume loss) on the cylindrical surface. Specifically, the cross-sectional area at the tail of the shield is about 0.5 to 0.6% smaller than the front shield. The reduction of the diameter occurs over the respective shield length, resulting in uniform contraction in each section. Due to slight overcutting, the annular void between the shield's extrados and the excavated ground may cause some slurry migration over a short distance behind the cutting wheel. However, predicting the actual overcut is challenging as it is highly dependent on workmanship, and this migration was not considered in the simulation.

In the numerical model, the shield does not share nodes with the surrounding ground, surface interaction is facilitated by interface elements, typically characterized as weaker and more flexible compared to the surrounding soil layer. Specifically, the interface was assumed to have smooth shear stiffness, with no friction forces reflecting the influence of the lubricants used around the shield.

4.3.3 Modeling EPB face pressure

The recorded face pressures in the excavation chamber were applied in front of the tunnel face. This face pressure was modeled by applying a pressure distribution perpendicular to the excavation face, using a segmental trapezoidal profile instead of the classical triangular earth pressure. This is due to the pressure loss from the screw conveyor in EPB tunneling. The decrease in pressure within the screw conveyor is unavoidable, as the pressure is reaching zero at the discharging outlet. According to Herrenknecht and Rehm [48], as reproduced in Fig.7, the pressure at the inlet of the screw conveyor has decreased to 80%, and the pressure gradient is contingent on the fluidity and impermeability of the mucks. The irregularity in pressure distribution arises from the difficulty in maintaining classical trapezoidal earth pressures during tunneling.

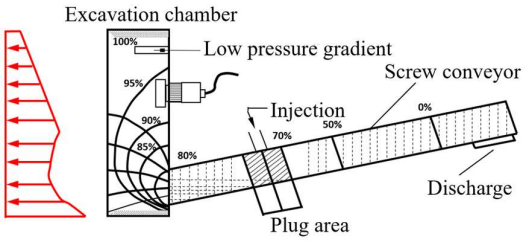

Fig.7 Earth pressure distribution diagram [48]

4.3.4 Modeling tail grouting pressure

As the TBM advances, cement grout is injected at the rear end of the shield to fill the annular gap - the space between the extrados of the segmental lining and the surrounding ground. The grout sets with time (hardening) while its stiffness increases. The time-dependent hardening response of grout material in shield tunneling has been investigated and presented by other researchers [8,9,11,49].

In the context of this study, tail void grouting was modeled with injection pressure over the periphery of the excavation, simulating the grout pressure in its fluid state. The grouting action was simulated using an isotropic, radially distributed pressure (perpendicular to the ground and increasing vertically) around a tunnel ring, as depicted in Fig.8. This distributional radial pressure has been adopted by other researchers [7,50]. Once again, the recorded grouting pressures were incorporated in the numerical modeling. It is essential to note that the grouting procedure is intricate, involving numerous uncertain parameters. However, this is beyond the scope of investigation in this paper.

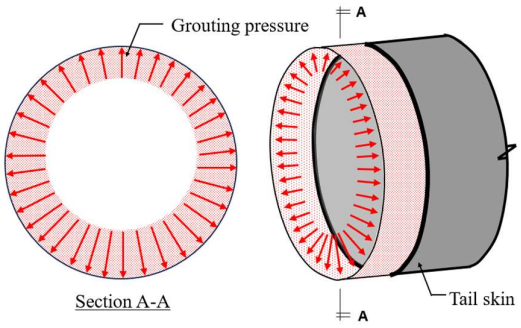

Fig.8 Profile of radial distribution grouting pressure increasing with depth adopted in the simulation

4.3.5 Modeling thrust jacking force

To advance during the boring process, the TBM must exert pressure against the existing tunnel lining. This is achieved through jack thrusting against the preceding lining.

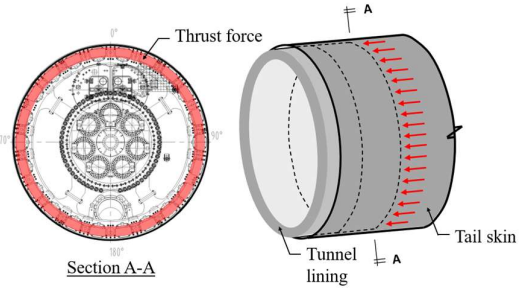

Fig.9 Simulated thrust jacking force over the cross-sectional surface of segmental lining

The recorded total thrust forces were simulated using distributed forces that directly act on the cross-sectional surface of the segments and have been assumed to be linear over the height of the tunnel, as illustrated in Fig.9.

4.3.6 Modeling segmental lining

The segmental lining is modeled as a continuous cylindrical shell, with the width and thickness of the segmental rings set at 1.4 m and 0.275 m respectively. This lining shell, positioned concentrically with the shield, is constructed at once. The tunnel lining properties adopted in the analysis are outlined in Table 5. The elastic parameters, including Young's modulus and Poisson's ratio are derived from the material characteristics of steel fiber reinforced concrete (SFRC) lining. A tunnel interface element is assigned to the tunnel extrados, with the interface strength reduction factor set to one in the case of the lining. The tunnel circumferences are assumed to be impermeable, disallowing any drainage into the tunnel lining.

Table 5 Material properties – SFRC tunnel lining

Parameter (unit)	Notation	Value
Type of material behaviour	-	Linear Elastic
Material type	-	Non-porous
Unit weight (kN/m^3)	γ	27.0
Young's modulus (kN/m^2)	E^{ref}	3.1 x 10^7
Poisson's ratio	ν	0.1
Interface strength reduction	R_{inter}	1.0

Kavvadas *et al.* [16] has confirmed that a continuous shell model serves as a reasonable approximation of linear elastic concrete segmental lining in the case of shallow or moderately deep tunnels, particularly when the stress levels in the tunnel lining are not excessively high. This assertion holds true under the assumption that both longitudinal and circumferential joints are infinitely stiff, thereby neglecting the influence of flexible joints. Similar observations have been made by earlier researchers [12,51,52]. In terms of

displacements, the continuum structure presents a realistic approach, as the joints' position rotates around the rings (i.e. staggered lining segments), and the total stiffness of the structure is nearly equivalent to a monolithic one [14]. However, it is crucial to acknowledge that a genuine simulation of the actual behavior of joints should be integrated into the structural analyses of segmental linings.

4.3.7 Simulation of the shield tunneling process

Shield tunneling encompasses multiple consecutive actions and construction stages, necessitating the representation of a repetitive pattern of sub-stages in the analysis. In finite element analysis, the tunneling process is typically simulated using the "element death" technique, allowing for the deactivation and activation of elements and nodes.

In the proposed numerical model, the TBM is initially activated in its starting position. Specifically, excavation slices with a total length equal to the shield length, are removed, and the water condition is set to dry in the excavated soil slices. Concurrently, support pressure is applied to the tunnel face. The first segmental ring is activated inside the shield without interacting with the surrounding shied component or the ground. It is important to note that the TBM is assumed to have already advanced into the ground for a certain length using the "all-in-once installation" method [36] in the initial step of the analysis. Subsequently, the following sub-stages are simulated in each excavation step:

(i) Advancing the excavation with prescribed displacements on the machine nodes by one ring length and removing the soil slice ahead of the current tunnel face.
(ii) Simultaneously removing the face pressure from the previous location and applying it to the new location (new excavation tunnel face).
(iii) Applying the thrust force exerted on the previously installed lining, causing the entire shield to move forward by one slice.
(iv) The segmental ring inside the shield is left behind, and another slice of lining is installed inside the machine.
(v) Applying a distributed surface load, equal to the grout injection pressure, on the exposed lining surface and excavated ground of equal length immediately after the tail of the shield.

This simulation approach is iteratively repeated to model the progressive advance of closed-face shield tunneling, aiming to achieve a realistic representation of EPB shield tunneling.

5. RESULTS AND DISCUSSION

5.1 Model Calibration and Validation

Before delving into the examination of how different modeling approaches impact tunneling-induced ground settlement, it is imperative to verify the accuracy of the results obtained with the developed numerical model. To achieve this, comparisons between the back-analyzed results and measured values are first employed for model calibration and validation.

In Fig.10, settlements measured on 30/10/2013, when the rear of the shield (Northbound TBM) passed the monitoring section, are presented. The back-analyzed results demonstrate a notably good agreement with the field measurement. Moreover, numerical analysis accurately predicts the magnitude and shape of the settlement trough induced by the tunnel excavation. The disparity between the numerical model results and the monitoring data was less than 10%, confirming the validation of the numerical model in terms of both the maximum ground settlement and the shape of the settlement trough.

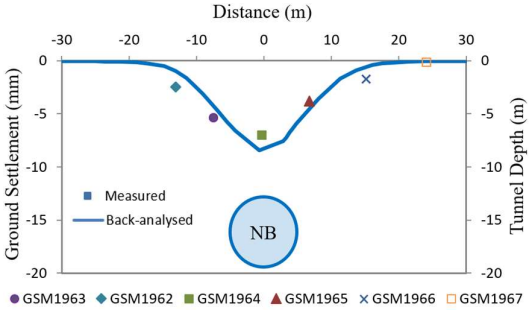

Fig.10 Validation of back-analyzed results for transverse settlement trough against field data

Similar to the approach taken for transverse settlements, Fig. 11 presents a comparison between the back-analyzed results and measured settlements over a period encompassing both the tunnel drives, from 25/10/2013 to 01/12/2013. Fundamentally, the surface settlement resulting from the excavation of the twin tunnels comprises two components: the surface settlement trough induced by the preceding tunnel and the trough caused by the following tunnel. The arrival of the TBM at and the passage of the tail shield through the monitoring section are denoted as the solid line and dotted line respectively, in Fig.11. Once again, a reasonably good agreement is observed between the back-analyzed results and the field measurement data, though some post-settlement rebound is evident in the field measurements immediately after the tail shied passed the monitoring section. There definitive

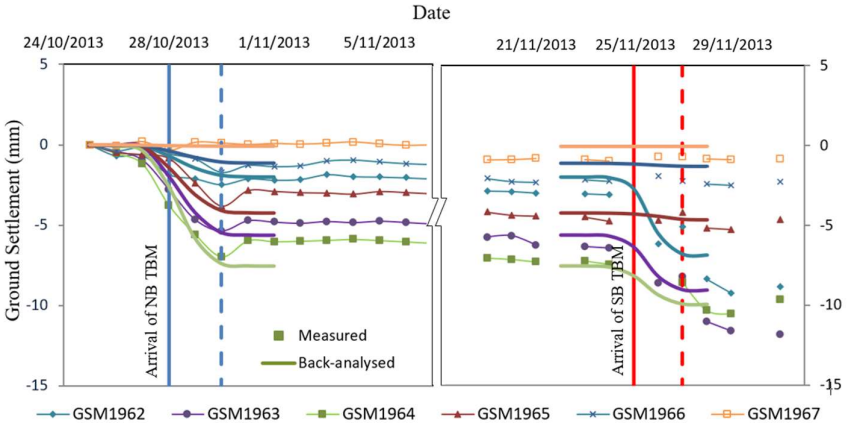

Fig.11 Measured and back-analyzed ground settlements over time

cause of this phenomenon remains unclear and could be attributed to factors such as measurement accuracy or localized soil conditions. Numerical analysis effectively predicts the trends and patterns of ground surface settlements resulting from the construction of the twin tunnels.

In Fig.11, it is apparent that the ground experiences additional settlements after the construction of the second tunnel. However, due to the absence of soil consolidation simulation in the analysis, the magnitude of long-term settlements is underestimated. Kasper and Meschke [9] highlighted that consolidation resulting from the dissipation of excess pore water pressure caused by tunneling is a significant factor contributing to long-term settlement.

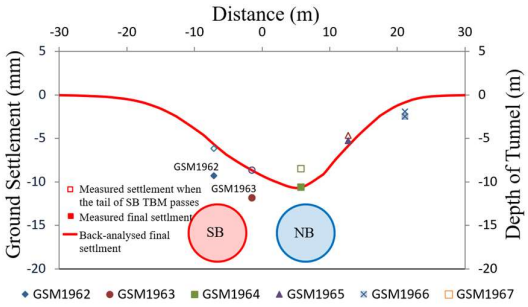

Fig.12 Measured and back-analyzed ground settlements after completion of both tunnels

Fig.12 illustrates the final settlement after simulating the construction of both tunnels, compared to the field measurements. The numerical analysis appears to under-predict the magnitude of subsequent settlements directly above the second tunnel (see GSM1962 and GSM1963). This discrepancy could potentially be attributed to the subsequent settlement caused by soil consolidation and/or disturbance of ground due to the shield driving, which could not be captured in the modeling. Prediction methods developed by Addenbrooke and Potts [53], and Hunt [54] have showed fairly good correlation with test data, particularly when accounting for the additional volume loss in the simulation of second tunnel construction.

5.2 Ground Surface Settlement Troughs

For the assessment of tunneling-induced ground surface settlement, measurements are commonly expressed through settlement troughs, whose shapes can be analyzed in terms of transverse and longitudinal axes of the tunnel separately. It is reasonably valid to assume that the transverse settlement profile exhibits a Gaussian shape, while the longitudinal profile takes the form of a cumulative probability curve, under the assumption that all ground deformation occurs at a constant volume [55]. This assertion has also been confirmed by Attewell and Woodman [56] based on numerous case histories of tunnel construction in clays.

From the numerical simulation, the development of the transverse settlement trough at monitoring section corresponding to Northbound TBM positions at -5D, -3D, -2D, -1D, monitoring section (MS), 1D, 2D, 3D and 5D is illustrated in Fig.13. The settlement trough conforms to a Gaussian distribution curve with a maximum ground settlement (S_{max}) of 9.57 mm, resulting in a settlement volume (V_s) of 0.5% and a trough width parameter (K) of 0.42. This trough with parameter falls within the typical range of 0.4 to 0.8 for residual soils of the Kenny Hill Formation [57].

According to O'Reilly and New [55], the distance from the tunnel axis to the inflection point (i) can be determined by the correlation between the trough width parameter (K) and tunnel depth (z_o). As observed in Fig.13, the width of the settlement trough is found to be 2.5i which tallies well with observations from various researchers [58,59].

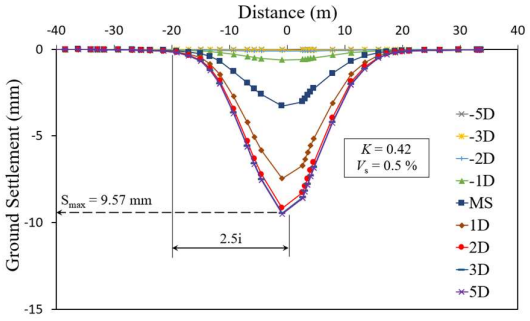

Fig.13 Simulated transverse ground surface settlement troughs

In Fig.14, the progressive longitudinal settlement troughs generated along the tunnel alignment are depicted from the numerical simulation. Taking the longitudinal settlement profile when the tunnel face is at monitoring section as an example, the surface settlement directly above the tunnel face is 3.76 mm, equivalent to 0.39S_{max}. This is considered reasonably valid for tunnels constructed with face support provided by compressed air. Field observations of settlements above EPB shield tunneling machines suggest that most of the construction settlement is associated with the tail void, and the surface settlement directly above the tunnel face is generally much less than 0.5S_{max} [60]. In contrast, for cases without face support, Attewell and Woodman [56] found that the surface settlement directly above the tunnel face generally corresponds to about 0.5S_{max} for tunnels constructed in stiff clays.

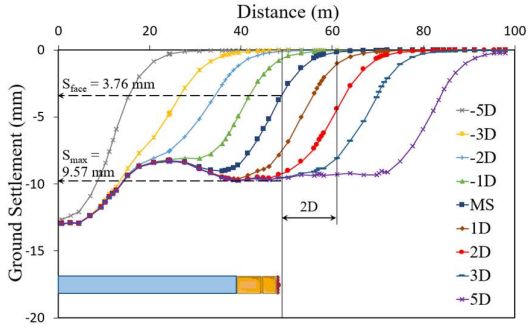

Fig.14 Simulated longitudinal ground surface settlement troughs

The numerical simulation reveals that the majority of settlements occur when the tunnel face is positioned 2D to 3D away. This aligns closely with field observations, where short-term settlements were typically found to be nearly complete when the shield tail had advanced 10 to 20 m (7 to 14 rings) beyond the monitoring section [34].

5.3 Settlement Influence Zone

The study highlights the formation of a typical settlement influence zone during shield tunnelling. For the Kenny Hill Formation, numerical verification demonstrates that the ground surface settlement remains insignificant beyond an offset of 2.5i from the tunnel center line. Additionally, ahead of the tunnel face, displacements are observed begin to mobilize at 2D distance, aligning closely with the concept of bearing pressure distribution for a circular footing to the tunnel face [61]. This concept suggests that approximately 90% of the differential strain induced by the face pressure is experienced within a two-diameter (2D) distance from the tunnel. This observation is supported by previous findings from Boon and Ooi [62].

Fig.15 provides a diagrammatical representation of the settlement influence zone derived from this study.

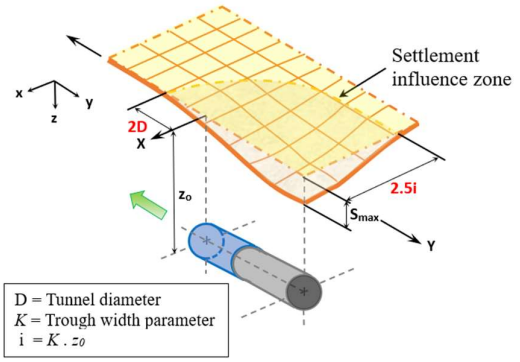

Fig.15 Settlement influence zone for shield tunneling in the Kenny Hill Formation

6. CONCLUSION

Mechanised shield tunneling is a complex multiparametric process, and correlating the parameters of a specific project to the assumptions of a methodology can be challenging. Therefore, there is a need for approaches that allow for realistic simulation of the tunneling process. This paper introduces such an approach and a numerical modeling technique that considers critical components and parameters of an EPB machine. The validity of these approaches is assessed using field measurements and TBM tunneling data collected from the KVMRT Kajang Line project.

A 3-D numerical model of the EPB shield tunneling process is developed using finite element code PLAXIS 3D, incorporating the importance findings from the data analysis of TBM key driving parameters. The back analysis results successfully validate the numerical model with a high accuracy against the field measurements of tunneling-induced

surface settlements. This study demonstrates that numerical simulation can realistically reproduce the main characteristics of EPB shield tunneling. The following state-of-the-art modeling techniques are recommended for a more accurate numerical simualtion:

(a) Non-linear face pressures with depth instead of the classical triangular earth pressure or a uniform distribution profile, and
(b) An effectively linear distributed pressure grouting pressure may be considered taking into account the grout weight and the increase of the stresses of the surrounding soil with depth.

From this validated numerical framework, settlement influence zone is established for the shield tunneling in the local ground condition, i.e. the Kenny Hill Formation, adding to the locally established tunneling data, such as volume loss, settlement trough parameters, etc., from the earlier works. Further exploration through systematic parametric studies is being conducted to analyze the influence and sensitivity of the various TBM driving parameters.

It is important to note that the recommendations and guidance provided with this work may not cover all possible cases, as they are derived from a limited number of numerical simulations. There is room for further improvement of the numerical simulation to capture additional aspects of the tunneling procedure that may be significant in certain cases. For instance, the need for coupled hydro-mechanical analysis to model the generation of excess pore water pressures caused by tunneling and subsequent consolidation over time, as well as the simulation of the resulted settlement through induced by the second tunnel in the case of twin tunnles, are recognized as some areas of future consideration and enhancement.

7. ACKNOWLEDGMENTS

The study presented in this paper is part of a research project funded by the Malaysian Ministry of Higher Education under the FRGS Grant 015MA0-154. The authors express their gratitude to the management of Mass Rapid Transit Corporation Sdn. Bhd. for granting permission to publish this paper and their positive support, which contributed to the success of this work. Special thanks are extended to Ir. Dr Lee Siew Wei of AECOM Hong Kong, whose insights and knowledge significantly contributed to this paper.

8. REFERENCES

[1] Janin J. P., Dias D., Emeriault F., Kastner R., Le Bissonnais H., and Guilloux, A., Numerical back-analysis of the southern Toulon tunnel measurements: A comparison of 3D and 2D approaches, Engineering Geology, 195, 2015, pp. 42-52.
[2] Maras-Dragojevic S., Analysis of ground settlement caused by tunnel construction, Casopis-Gradjevinar.Hr, 64, 2012, pp. 573-581.
[3] Möller S., Tunnel induced settlements and structural forces in linings, PhD thesis, Stuttgart: Institute of Geotechnical Engineering, Universitat of Stuttgart, 2006.
[4] Lin D. G., Tseng C. T., Phienwej N., and Suwansawat S., 3-D deformation analysis of earth pressure balance shield tunnelling in Bangkok subsoil, Journal of Southeast Asian Geotechnical Society, 2002, pp. 13-27.
[5] Lim K. C., Three-dimensional finite element analysis of earth pressure balance tunnelling, PhD thesis, National University of Singapore, 2003.
[6] Ng C. W. W., Lee G. T. K., and Tsang D. K. W., 3D numerical investigations of NATM twin tunnel interactions, Canadian Geotechnical Journal, Vol. 41, No. 3, 2004, pp. 523-539.
[7] Kasper T. and Meschke G., A 3D finite element simulation model for TBM tunnelling in soft ground, International Journal for Numerical and Analytical Methods in Geomechanics, Vol. 28, Issue 14, 2004, pp. 1441-1460.
[8] Kasper T. and Meschke G., A numerical study of the effect of soil and grout material properties and cover depth in shield tunnelling, Computers and Geotechnics, Vol. 33, Issue 4-5, 2006, pp. 234-247.
[9] Kasper T. and Meschke G., On the influence of face pressure, grouting pressure and TBM design in soft ground tunnelling, Tunnelling and Underground Space Technology, Vol. 21, Issue 2, 2006, pp. 160-171.
[10] Zhao K., Janutolo M., and Barla G., A completely 3D model for the simulation of mechanized tunnel excavation, Rock Mechanics and Rock Engineering, Vol. 45, Issue 4, 2012, pp. 475-497.
[11] Lambrughi A., Medina Rodriguez L., and Castellanza R., Development and validation of a 3D numerical model for TBM-EPB mechanized excavations, Computers and Geotechnics, Vol. 40, 2012, pp. 97-113.
[12] Do N. A., Dias D., Oreste P., and Djeran-Maigre I., Three-dimensional numerical simulation for mechanized tunnelling in soft ground: the influence of the joint pattern, Acta Geotechnica, 2013, pp. 1-22.
[13] Do N. A., Dias D., Oreste P., and Djeran-Maigre I., Three-dimensional numerical simulation of a mechanized twin tunnels in soft ground, Tunnelling and Underground Space Technology, Vol. 42, 2014, pp. 40-51.
[14] Litsas D., Rachmani A., Fortsakis P., and Kavvadas M., 3D numerical simulation of shield

tunnelling with emphasis on the influence of the tail gap, in Proceedings of the 2nd Eastern European Tunnelling Conference, Athens, Greece, 2014, pp. 1-9.
[15] Fargnoli V., Gragnano C. G., Boldini D., Amorosi A., 3D numerical modelling of soil-structure interaction during EPB tunnelling, Géotechnique, Vol. 65, Issue 1, 2015, pp. 23-27.
[16] Kavvadas M., Litsas D., Vazaios I., and Fortsakis P., Development of a 3D finite element model for shield EPB tunnelling, Tunnelling and Underground Space Technology, Vol. 65, 2017, pp. 22-34.
[17] Vitali O. P. M., Celestino T. B., and Robet A., 3D finite element modelling optimization for deep tunnels with material nonlinearity, Underground Space, Vol. 3, 2017, pp. 125-139.
[18] Nikakhtar L., Zare sh., and Mirzaei-Nasirabad H., Numerical modelling of backfill grouting approaches in EPB tunnelling, Journal of Mining and Environment, Vol. 11, No. 1, 2020, pp. 301-314.
[19] Founta V., Ninic J., Whittle A. J., Meschke G., and Stascheit J., Numerical simulation of ground movements due to EPB tunnelling in clay, in Proceedings of the 3rd International Conference on Computational Methods in Tunnelling, 2013, pp. 97-108.
[20] Namazi E., Mohamad H., Jorat M. E., and Hajihassani M., Investigation on the effects of twin tunnel excavations beneath a road underpass, Electronic Journal of Geotechnical Engineering, Vol. 16, Issue 1, 2011, pp. 1-8.
[21] Namazi E., Mohamad H., Kueh A. B. H., Hajihassani M., Jusoh S. N., and Khaili Abad S. V. A. N., Ground behaviour around a tunnel using various soil models, Electronic Journal of Geotechnical Engineering, Vol. 17, 2012, pp. 609-622.
[22] Billota E., Paolillo A., Russo G., and Aversa S., Displacements induced by tunnelling under a historical building, Tunnelling and Underground Space Technology, Vol. 61, 2017, pp. 221-232.
[23] Kratz B., Jehel P., and Tatin M., 3D numerical simulation of TBM excavation for predicting surface settlements – state of the art, Expanding Underground, Knowledge and Passion to Make a Positive Impact on the World – Anagnostou, Benardos & Marinos (Eds), 2023, pp. 2757-2765.
[24] Chortis F., Tzivakos K., and Kavvadas M., Investigation of the influence of face pressure on surface settlements in EPB mechanized tunnelling, in Proceedings of the 2nd Eastern European Tunnelling Conference, Athens, Greece, 2014, pp. 1-10.
[25] Nagel F. and Meschke G., Grout and bentonite flow around a TBM: Computational modeling and simulation-based assessment of influence on surface settlement, Tunnelling and Underground Space Technology, Vol. 26, 2011, pp. 445-452.
[26] Muir Wood, A. N., The circular tunnel in elastic ground, Géotechnique, Vol. 25, Issue 1, 1975, pp. 115-127.
[27] Arnau O. and Molins C., Three-dimensional structural response of segmental tunnel linings, Engineering Structures, Vol. 44, 2012, pp. 210-221.
[28] Gomes R. A. M. P. and Celestino T. B., Influence of physical and geometrical parameters on three-dimensional load transfer mechanism at tunnel face, Canadian Geotechnical Journal, Vol. 46, Issue 7, 2009, pp. 855-868.
[29] Meisnerr H., Tunnelbau unter tage – Empfelunghen des Arbeit-skreises, Geotechnik, Vol. 19, Issue 2, 1996, pp. 99-108.
[30] Vlachopoulos N. and Diederichs M. S., Appropriate uses and practical limitations of 2D numerical analysis of tunnels and tunnel support response, Geotechnical and Geological Engineering, Vol. 32, Issue 2, 2014, pp. 469-488.
[31] Ramsheh F. A., Rashiddel A., and Dias D., 3D numerical simulations of tunneling induced soil deformations, Journal of Physics: Conference Series, Vol. 1973, 012207, 2021, pp. 1-8.
[32] Khoo C. M., Effects of earth pressure balance shield tunnelling on ground settlement, MSc thesis, Universiti Teknologi PETRONAS, 2020.
[33] Chin R. M., Salehudin M. S., and Abdullah Husairi N., Performance of EPB tunnelling in Kenny Hill Formation, in Proceedings of International Conference and Exhibition on Tunnelling and Underground Space (ICETUS 2015), Kuala Lumpur, Malaysia, 2015, pp. 298-301.
[34] Khoo C. M., Gopalan T., Abdul Rahman, N. A., and Terry A. W., Effects of EPB shield tunnelling on ground surface settlements – A case study in Kenny Hill Formation, in Proceedings of ITA-AITES World Tunnel Congress (WTC 2020), Kuala Lumpur, Malaysia, 2020, pp. 623-627.
[35] Vermeer P. A. and Brinkgreve R., PLAXIS Manual, AA Balkema, Rotterdam, 1993.
[36] Vermeer P. A., Bonnier P. G., and Möller S. C., On a smart use of 3D-FEM in tunnelling, 2002.
[37] Maleki M. and Nabizadeh A., Seismic performance of deep excavation restrained by guardian truss structures system using quasi-static approach, SN Applied Sciences, Vol. 3, 417, 2021.
[38] Maleki M. and Mohammad Hosseini S. M. M., Assessment of the Pseudo-static seismic behavior in the soil nail walls using numerical analysis, Innovative Infrastructure Solutions, Vol. 7, 262, 2022.
[39] Khoo C. M., Influence of 3-D model geometry on numerical simulation of tunnelling effects, in Proceedings of Southeast Asian Conference and

Exhibition on Tunnelling and Underground Space (SEACETUS 2024), Kuala Lumpur, Malaysia, 2024, pp. 195-200.
[40] Benz T., Small-strain stiffness of soils and its numerical consequences, PhD thesis, Universitat Stuttgart, 2007.
[41] Duncan J. M. and Chang C. Y., Nonlinear analysis of stress and strain in soil, Journal of Soil Mechanics and Foundations, Div ASCE96, 1970, pp. 1629-1653.
[42] Schanz T., Vermeer P. A., and Bonnier P. G., The hardening soil model: Formulation and verification, 2019.
[43] Atkinson J. H., Non-linear soil stiffness in routine design, 40th Rankine Lecture, Géotechnique, Vol. 50, Issue 5, 2000, pp. 487-508.
[44] Tan Y. C., Liew S. S., Gue S. S., and Taha M. R., A numerical analysis of anchored diaphragm walls for a deep basement in Kuala Lumpur, Malaysia, in Proceedings of the 14th Southeast Asian Geotechnical Conference, Hong Kong, 2001.
[45] Govindasamy D., Mohamad Ismail M. A., Mohamad Zaki M. F., and Zainal Abidin M. H., Calibration of stiffness parameters for Hardening Soil model in residual soil from Kenny Hill formation, Bulletin of the Geological Society of Malaysia, Vol. 67, 2019, pp. 119-125.
[46] Veeresh C., Goh K. H., and Wen D., Characterising the small strain stiffness behaviour of the Singapore old alluvium, in Proceedings of 15th Asian Regional Conference on Soil Mechanics and Geotechnical Engineering, Fukuoka, Japan, 2015, pp. 581-586.
[47] Lee S. W., Choy C. K. M., Tse S. C., van Gool F. R., Cheang W. W. L., and Brinkgreve R. B. J., 3D numerical modelling of tunnelling intersecting piles, Geotechnical Aspects of Underground Construction in Soft Ground, Viggiani (ed), Taylor & Francis Group, London, 2012, pp. 919-925.
[48] Herrenknecht M. and Rehm U., Earth pressure balanced shield technology, Internal Lecture in Colorado School of Mine, USA, 2003.
[49] Ramoni M., Lavdas N., and Anagnostou G., Squeezing loading of segmental linings and the effect of backfilling, Tunnelling and Underground Space Technology, Vol. 26, Issue 6, 2011, pp. 692-717.
[50] Mollon G., Dias D., and Soubra A., Probabilistic analyses of tunnelling-induced ground movements, Acta Geotechnica, Vol. 8, 2013, pp. 181-199.
[51] Litsas D., Fortsakis P., and Kavvadas M., 3D simulation of mechanized tunnel excavation, in Proceedings of the 3rd Arabian Tunnelling Conference & Exhibition, Dubai, UAE, 2015.
[52] Klappers G., Grübl F., and Ostermeier B., Structural analyses of segmental lining – coupled beam and spring analyses versus 3D-FEM calculations with shell elements, Tunnelling and Underground Space Technology, Vol. 21, 2006, pp. 254-255.
[53] Addenbrooke T. I. and Potts D. M., Twin tunnel interaction – surface and subsurface effects, International Journal of Geomechanics, Vol. 1, 2001, pp. 249-271.
[54] Hunt D. V. L., Predicting the ground movements above twin tunnels constructed in London Clay, PhD thesis, University of Birmingham, 2005.
[55] O'Reilly M. P. and New B. M., Settlement above tunnels in the United Kingdom – their magnitude and prediction, Tunnelling 82, IMM, London, 1982, pp. 173-181.
[56] Attewell P. B. and Woodman J. P., Predicting the dynamics of ground settlement and its derivatives caused by tunnelling in soil, Ground Engineering, Vol. 15, No. 8, 1982, pp. 13-22.
[57] Khoo C. M., Gopalan T., Abdul Rahman N. A., and Mohamad H., Volume loss caused by tunnelling in Kenny Hill Formation, International Journal of GEOMATE, Vol. 16, Issue 54, 2019, pp. 164-169.
[58] Peck R. B., Deep excavation and tunnelling in soft ground – state-of-the-art report, in Proceedings of the 7th International Conference on Soil Mechanics and Foundations Engineering, Mexico, 1969, pp. 225-290.
[59] Cording E. J. and Hansmire W. H., Displacements around soft ground tunnels, General Report, 5th Pan-American Conference on Soil Mechanics and Foundations Engineering, Buenos Aires, 1975, pp. 571-632.
[60] Mair R. J. and Taylor R. N., Theme lecture: Bored tunnelling in the urban environment, in Proceedings of the 14th International Conference on Soil Mechanics and Foundation Engineering, Hamburg, 1997, pp. 2353-2385.
[61] Loganathan N., Design charts: Tunnelling-induced effects on adjacent pile foundation, in Proceedings of the 19th Southeast Asian Geotechnical Conference & 2nd AGSSEA Conference, Kuala Lumpur, Malaysia, 2016, pp. 1125-1130.
[62] Boon C. W. and Ooi L. H., Longitudinal and transverse interactions between stacked parallel tunnels constructed using shield tunnelling in residual soil, Geotechnical Engineering Journal of the SEAGS & AGSSEA, Vol. 49, No. 2, 2018, pp. 57-71.